Molecular Basis for the Binding of Competitive Inhibitors of Maize Polyamine Oxidase†

Alessandra Cona,‡,§ Fabrizio Manetti,§,|| Rosalida Leone,|| Federico Corelli,|| Paraskevi Tavladoraki,‡ Fabio Polticelli,‡ and Maurizio Botta*,||

Dipartimento di Biologia, Università "Roma Tre", Viale Guglielmo Marconi 446, I-00146 Roma, Italy, and Dipartimento Farmaco Chimico Tecnologico, Università degli Studi di Siena, I-53100 Siena, Italy

Received December 1, 2003; Revised Manuscript Received January 16, 2004

ABSTRACT: Maize polyamine oxidase (MPAO), the only member of the polyamine oxidase (PAO) family whose three-dimensional structure is known, is characterized by a 30 Å long U-shaped catalytic tunnel located between the substrate binding domain and the FAD. To shed light on the MPAO ligand binding mode, we studied the inhibition properties of linear diamines, agmatine, prenylagmatine (G3), G3 analogues, and guazatine, and analyzed the structural determinants of their biological activity. Linear diamines competitively inhibited MPAO, with the inhibitory activity increasing as a function of the number of methylene groups. With regard to the guanidino competitive inhibitors, including agmatine, G3, and G3 analogues, the presence of a hydrophobic substituent constitutes the principal factor influencing MPAO inhibition, as the addition of a hydrophobic substituent to the guanidino group of both G3 and G3 analogues greatly increases the inhibitory activity. Moreover, results obtained by a molecular modeling procedure indicated that in their preferred orientation, G3 analogues point the ammonium group toward the narrow entrance of the tunnel, while the terminal hydrophobic group is located within the large entrance. The high binding affinity for MPAO exhibited by G3 and G3 analogues bearing a prenyl group as a substituent on the guanidino moiety is in agreement with the observation that the prenyl group binds in a well-defined hydrophobic pocket, mainly formed by aromatic residues. Finally, docking simulations performed with the charged and uncharged forms of MPAO inhibitors indicate that the stereoelectronic properties of the MPAO active site are consistent with the binding of inhibitors in the protonated form.

PAOs[1] are FAD-containing enzymes which oxidize polyamines at the secondary amino group into various products, depending on the taxa. Plant, bacterial, and protozoan PAOs are responsible for the terminal catabolism of polyamines, transforming spermidine (spd) and spermine (spm) into 4-aminobutyraldehyde and 3-(aminopropyl)-4-aminobutyraldehyde, respectively, in addition to 1,3-diaminopropane. Conversely, animal PAOs are involved in the interconversion metabolism of polyamines, transforming spd and spm into putrescine (put) and spd, respectively, with 3-aminopropionaldehyde (*1*). The overall reaction catalyzed by PAOs can be divided into a reductive half-reaction, in which the flavin is reduced upon polyamine oxidation, and an oxidative half-reaction, in which the reduced flavin is reoxidized by molecular oxygen with the release of hydrogen peroxide. Polyamine oxidation results in the formation of an imino compound, which is hydrolyzed to yield the final products. Notwithstanding the possible differences in the mechanistic details of the enzyme reaction, PAOs constitute a homogeneous group of enzymes sharing similar biochemical properties (*2*).

In the past, PAOs have been thought to be mainly involved in polyamine homeostasis, these basic molecules being well-known regulators of cell growth and cycle progression (*3*). However, recently there has been a growing interest in the role of polyamine catabolic products, especially hydrogen peroxide and aminoaldehydes which are both considered strong inducers of apoptosis (*3*). In this respect, it has been demonstrated that the antitumoral effect exhibited by some polyamine analogues in sensitive cells may be due in part to the oxidative stress resulting from the accelerated polyamine catabolism, besides downregulation of their biosynthesis (*4*). Therefore, the modulation of both polyamine intracellular levels and catabolism appears to be a general mechanism regulating cell growth and death. In plants, polyamine catabolism has been thought to be involved in cell wall strengthening processes during different physiological events and cellular defense (*5*, *6*). In this regard, a growing body of evidence suggests that cell wall stiffening *in vivo* is controlled by the synthesis of hydrogen peroxide (*7*) and maize (*Zea mays* L.). PAO (MPAO) has been proposed to be a candidate for hydrogen peroxide production in the outer tissue of maize mesocotyl during de-etiolation (*8*).

MPAO is the only PAO for which the tertiary structure has been determined (*9*). Molecular modeling of barley PAO (BPAO) (*10*) and mouse spermine oxidase (*2*), based on the

† This work was supported by grants to M.B. from the Italian MIUR (2002038577) and from the Merck Research Laboratories (2002 Academic Development Program Chemistry Award).

* To whom correspondence should be addressed: Dipartimento Farmaco Chimico Tecnologico, Università degli Studi di Siena, Via Aldo Moro, I-53100 Siena, Italy. Phone: +39 0577 234306. Fax: +39 0577 234333. E-mail: botta@unisi.it.

‡ Università "Roma Tre".

§ These authors contributed equally to this work.

|| Università degli Studi di Siena.

[1] Abbreviations: MPAO, maize polyamine oxidase; PAO, polyamine oxidase; G3, prenylagmatine; spd, spermidine; spm, spermine; put, putrescine; MDL72527, *N*,*N*′-bis(2,3-butadienyl)-1,4-butanediamine; BPAO, barley polyamine oxidase; SPMC, statistical pseudo-Monte Carlo.

10.1021/bi036152z CCC: $27.50
Published on Web 03/02/2004

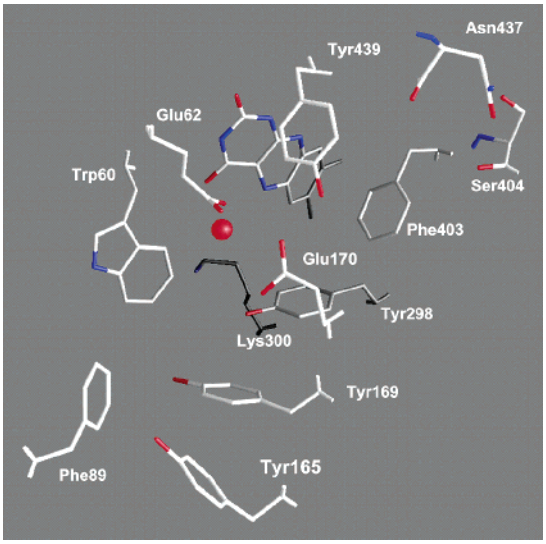

FIGURE 1: Schematic representation of the active site of maize PAO (PDB entry 1B37) (*9*) showing the residues composing the catalytic tunnel. For the sake of clarity, only the isoalloxazine ring of FAD is shown. The water molecule bridging through hydrogen bonds of the FAD N5 atom and the amino group of Lys300 is represented by a red sphere. The backbone of residues Asn437 and Ser404, whose carbonyl groups line the narrow tunnel entrance, is also shown.

three-dimensional structure of MPAO, suggests that the general features of the MPAO active site are conserved in both enzymes. Thus, MPAO represents an important model protein for the study of the polyamine oxidase catalytic mechanism and for the design of new inhibitors for both plant and animal PAOs.

The crystal structure of the native MPAO in the oxidized and reduced state, as well as in complex with the inhibitors *N*,*N*′-bis(2,3-butadienyl)-1,4-butanediamine (MDL72527), 1,8-diaminooctane, guazatine, and N^1-ethyl-N^{11}-[(cycloheptyl)methyl]-4,8-diazaundacane (*9*, *11*), revealed a 30 Å long U-shaped catalytic tunnel located at the interface between the substrate binding domain and the FAD binding domain (Figure 1). The innermost part of the tunnel is positioned in front of the flavin isoalloxazine ring and forms the catalytic center. A ring of solvent-accessible glutamate and aspartate side chains surrounding one of the two tunnel openings may help to steer the polycationic substrate toward the tunnel interior. The tunnel is lined mainly by carboxylate and aromatic side chains. In particular, the side chains of Glu62 and Glu170 protrude in front of the flavin and are within hydrogen bonding distance of one another and of active site ligands. The Glu62−Glu170 pair may represent the structural element that properly aligns the substrate within the tunnel (*11*). Aromatic residues such as Phe403, Tyr439, and Tyr298 are also crucial elements of the catalytic tunnel. The side chains of Phe403 and Tyr439 are positioned parallel to each other and flank the tunnel on opposite sites, forming a kind of aromatic sandwich which establishes interactions with enzyme-bound inhibitors (Figure 1). The Tyr298 side chain also appears within hydrogen bonding distance of active site ligands. A striking feature of MPAO is that the catalytic tunnel is embedded by carbonyl and carboxylated oxygen atoms which extensively interact with active site-bound inhibitors (*9*). Furthermore, the determination of the three-dimensional structure of inhibitor-bound MPAO (*9*, *11*) revealed that ligand binding in the catalytic site does not induce any significant conformational change, but leads to the formation of a solvent-inaccessible environment in which a single water molecule, bridging the ammonium group of Lys300 and the flavin N5 atom, is trapped (Figure 1). It is worth mentioning that Lys300 is the only active site residue whose conformation changes upon FAD reduction, probably to compensate for the change in the flavin protonation state (*11*). Despite the knowledge of the structural details of the active site, little is known about the catalytic mechanism of MPAO. In particular, an important issue is represented by the protonation state of the substrates within the tunnel. In fact, the presence of a polycationic molecule in a solvent-inaccessible environment would give rise to strong electrostatic effects which in turn could play a major role in catalysis.

Strong and specific PAO inhibitors may represent important tools in unraveling the catalytic mechanism of PAO and in designing new antineoplastic drugs. They may also be valuable tools in studying the physiological role of this class of enzymes in both plant and animal cell growth and differentiation. Guazatine is the most powerful plant PAO inhibitor presently available, inhibiting MPAO with a K_i value of 7.5 nM (*12*). However, the well-known toxicity of this compound, commonly used as a fungicide in agriculture, makes it as an unsuitable tool for physiological studies. Recently, it has been reported that the natural compound *N*-prenylagmatine (G3, Figure 2), a hypotensive agent isolated from *Verbesina caracasana* (*13*), is able to inhibit both pig liver PAO and MPAO (*12*). G3 analogues (Figure 2), hereafter termed Ro inhibitors, have also been synthesized and tested for MPAO and BPAO inhibition activities (*14*).

In the study presented here, we carried out a detailed analysis of the properties of linear diamines as *in vitro* inhibitors of MPAO enzyme activity and of the structural basis for their activity. Moreover, the MPAO inhibition properties of agmatine, G3, Ro inhibitors, and guazatine are compared to those of linear diamines and critically revised on the basis of the enzyme three-dimensional structure. In addition, on the basis of the three-dimensional structure of the complex between MPAO and guazatine (*11*), a computational protocol consisting of molecular docking, conformational analysis, and energy minimization procedures has been used to analyze the process by which the enzyme recognizes the inhibitors, and to evaluate the interaction pathways between MPAO and inhibitors in the computationally generated complexes. The reliability of the computational approach has been tested on the prediction of the geometry of binding of 1,8-diaminooctane to MPAO, yielding results in agreement with the available three-dimensional structure of the MPAO−1,8-diaminooctane complex (*11*). Using this molecular mechanics approach, different modes of binding of each inhibitor into the U-shaped catalytic tunnel of MPAO were found, in agreement with what was reported for 1,8-diaminooctane. Moreover, docking simulations carried out with the charged and uncharged forms of MPAO inhibitors indicated that the stereoelectronic properties of the MPAO active site were consistent with the binding of inhibitors in the protonated form, a feature which can shed light on the still obscure MPAO catalytic mechanism.

EXPERIMENTAL PROCEDURES

Enzyme Activity and Inhibition Assays. MPAO was purified as previously described (*15*). Enzyme activity was

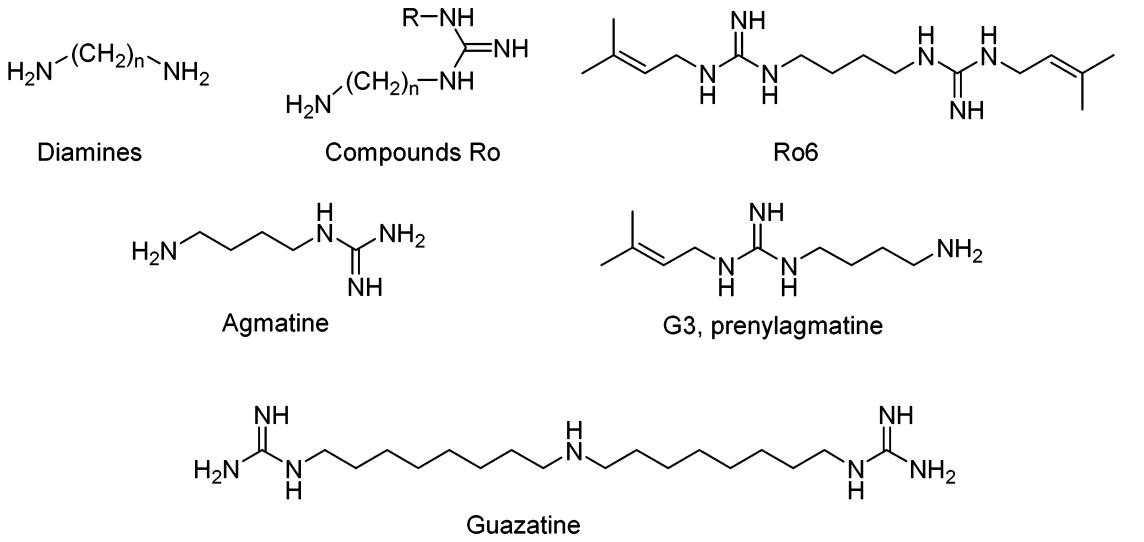

Compounds. Diamines: 1,3-diaminopropane, n = 3; 1,4-diaminobutane, n = 4; 1,5-diaminopentane, n = 5; 1,6-diaminohexane, n = 6; 1,7-diaminoheptane, n = 7; 1,8-diaminooctane, n = 8; 1,9-diaminononane, n = 9; 1,10-diaminodecane, n = 10; 1,12-diaminododecane, n = 12. **Ro derivatives**: Ro1, n = 4, R = allyl; Ro2, n = 4, R = *p*-fluorobenzyl; Ro3, n = 4, R = propargyl; Ro4, n = 5, R = isoprenyl; Ro5, n = 6, R = isoprenyl.

FIGURE 2: Chemical structures of diamines, agmatine, G3 (prenylagmatine), G3 analogues (Ro compounds), and guazatine.

measured spectrophotometrically by following the formation of a pink adduct ($\epsilon_{515} = 2.6 \times 10^4$ M^{-1} cm^{-1}) as a result of the oxidation and subsequent condensation of aminoantipyrine and 3,5-dichloro-2-hydroxybenzenesulfonic acid catalyzed by horseradish peroxidase (*16*). Activity assays were carried out in 0.2 M sodium phosphate buffer (pH 6.5), using spermidine as a substrate, in the absence and presence of diamines. Enzyme activities were expressed in units (1 unit is the amount of enzyme that catalyzes the oxidation of 1 μmol of substrate per minute). In the enzyme assays, the MPAO concentration ranged from 2.0 to 4.0 nM (i.e., [E] < [S] and [E] < [I], where [E], [S], and [I] represent the enzyme, substrate, and inhibitor concentrations, respectively), while the substrate concentration ranged from $0.1K_m$ to $10K_m$ (where K_m is the Michaelis constant). Moreover, the inhibitor concentration ranged from $0.1K_i$ to $10K_i$ (where K_i is the apparent dissociation equilibrium constant for the formation of the reversible enzyme−inhibitor complex). Under all the experimental conditions, the initial reaction rate for the enzyme-catalyzed conversion of the substrate was unaffected by the incubation time for the enzyme−inhibitor complex, prior to substrate addition. In fact, the enzyme−inhibitor equilibration time was very short, being complete within the mixing time (e.g., 15 s). K_i values were determined according to the Dixon graphical method (*17*). The data that are reported are the average of values obtained in three different experiments, each with two replicates. The standard error for each point was less than 8%. All data were obtained at 25 °C.

Molecular Modeling of the Enzyme−Inhibitor Complexes. All calculations and graphical manipulations were performed on Silicon Graphics computers (Origin 300 server and Octane workstations) using the software package MacroModel/BatchMin (*18*, *19*) equipped with the AMBER* united-atoms force field (*20*).

The MPAO atomic coordinates used in the modeling studies were derived from the structure of the complex of MPAO and guazatine, refined at 1.9 Å resolution [Protein Data Bank entry 1H82 (*11*)].

To create the initial coordinates for the docking studies, the α-D-fucose, the two α-D-mannose, and the two *N*-acetyl-D-glucosamine residues present in the crystal structure of MPAO were removed and excluded from all the calculations. Similarly, the crystallographic water molecules were removed from the guazatine−MPAO complex, with the exception of the following molecules which were considered in all the calculations: (i) the molecule labeled as HOH158, present in the oxidized enzyme in the proximity of Lys300 and the N5 atom of FAD and constituting the so-called Lys300/water/flavin N5 motif; (ii) the molecules labeled HOH253 and HOH94, found at the entrances of the catalytic site in the proximity of Asn437 and Tyr165, respectively; and (iii) molecules HOH10, HOH23, HOH232, HOH264, HOH265, and HOH266, located in the FAD binding site.

Hydrogen atoms were added to their idealized positions at pH 6.5 using InsightII (version 2000) Biopolymer software (*21*), to protonate all the guanidino and amino groups of Arg and Lys residues, as well as both the N-terminal primary amino group and the guanidino moieties of the inhibitors, and to deprotonate all the carboxy groups of Glu and Asp side chains, as well as the C-terminal carboxy group.

The atomic partial charges for the enzyme were taken from the AMBER* force field, while those for the FAD and the inhibitors were calculated with MOPAC (*22*) using the MNDO approximation.

In the study presented here, the computational step corresponding to the molecular docking approach is simplified, since the topography of the enzyme active site, as well as the binding mode of several enzyme inhibitors, such as 1,8-diaminooctane and guazatine, is known (*11*). Thus, the docking problem is essentially reduced to locate the possible

conformations of the inhibitor(s) within the active site of the enzyme.

The three-dimensional structure of the MPAO−guazatine complex was used as a template to model the complexes between MPAO and G3 analogues. In detail, the guanidino moiety of Ro4, taken as a representative compound of all the G3 analogues, was superimposed arbitrarily onto the corresponding group of guazatine located at the narrow entrance of the catalytic tunnel. Dihedral angles of Ro4 were then manually modified to fit the inhibitor structure to the guazatine conformation.

The same protocol was used to model the structure of 1,8-diaminooctane on the guazatine template. Such a simulation has been performed with the aim of testing the ability of our computational approach to exhaustively investigate the possible orientations of inhibitors inside the U-shaped catalytic tunnel of MPAO.

The complexes that were generated were then submitted to a statistical conformational search consisting of 10 000 steps of the Statistical Pseudo Monte Carlo (SPMC) method involving all the rotatable bonds of the inhibitors. It is important to note that the conformational mobility of the active site residues was not a complicating factor since it has been shown that these residues undergo only minor structural changes upon the binding of different inhibitors. Moreover, the BatchMin command MOLS was applied to allow for rotation and translation of inhibitors inside the catalytic tunnel, with a maximum value for the random rotational angle set to 180° and a maximum allowed translational movement of 3.0 Å at each step.

Solvation conditions were simulated using a continuum approach, instead of a large number of explicit solvent molecules (*23*). To ensure that the ligand remained in the catalytic tunnel during the docking simulations, a constraint was imposed on the distance between the terminal amino group of the inhibitors and the flavin N5 atom of MPAO, the minimum and maximum allowed distances being 2.5 and 11 Å, respectively. Moreover, because of the large number of atoms in the model, to correctly optimize the MPAO−inhibitor complexes obtained by the flexible docking and conformational search procedures, the following additional constraints had to be imposed.

(i) A subset, comprising only the inhibitor and a shell of residues possessing at least one atom 5 Å from any of the inhibitor atoms, was created and subjected to energy minimization. The inhibitor and all the amino acid side chains of the shell were unconstrained during energy minimization to allow for reorientation and proper hydrogen bonding geometries and van der Waals contacts. (ii) All the atoms not included in the above-defined subset were fixed, but their nonbond interactions with all the relaxing atoms have been calculated.

Energy minimization of the complexes was performed using the steepest descent method until the derivative convergence was 0.01 kcal $Å^{-1}$ mol^{-1}.

GRID Calculations. The program GRID (version 16) (*24*, *25*) maps the protein onto a three-dimensional grid and calculates for each grid point the interaction energy (including contributions from the van der Waals, electrostatic, and hydrogen bond interactions) between a probe and all the protein atoms. The MPAO coordinates were converted into an input structure for GRID using the program GRIN, also implemented in the GRID package. GRIN checks the input structure for errors and assigns to each atom appropriate parameters necessary for the GRID calculations.

The probes that were used were DRY (hydrophobic probe), N2 (sp^3 NH_2 with a lone pair), and N3+ (sp^3 amine NH_3 cation). A value of 0 was used for the GRID keyword MOVE, thus allowing lone pairs and tautomeric hydrogen atoms to move in response to the probe.

Table 1: MPAO Inhibitory Activity Values (K_i) of Diamines, Agmatine, Prenylagmatine (G3), G3 Analogues (Ro Compounds), and Guazatine

inhibitor	K_i (M)[a]
1,3-diaminopropane[b]	1.0×10^{-4}
1,4-diaminobutane[b]	1.3×10^{-4}
1,5-diaminopentane[b]	3.8×10^{-5}
1,6-diaminohexane[b]	3.0×10^{-6}
1,7-diaminoheptane[b]	4.0×10^{-7}
1,8-diaminooctane[b]	3.0×10^{-7}
1,9-diaminononane[b]	1.2×10^{-6}
1,10-diaminodecane[b]	6.0×10^{-7}
1,12-diaminododecane[b]	1.7×10^{-7}
agmatine[c]	3.0×10^{-6}
prenylagmatine (G3)[c]	1.5×10^{-8}
Ro1[d]	1.3×10^{-7}
Ro2[d]	6.3×10^{-7}
Ro3[d]	2.5×10^{-7}
Ro4[d]	1.0×10^{-8}
Ro5[d]	2.2×10^{-8}
Ro6[d]	1.5×10^{-6}
guazatine[c]	7.5×10^{-9}

[a] K_i values are means of three different experiments, each performed in duplicate. The standard error for each point was less than 8%. [b] From this study. [c] From ref *12*. [d] From ref *14*.

RESULTS

Analysis of MPAO Inhibition Properties of Linear Diamines, Agmatine, G3, G3 Analogues, and Guazatine

Diamines. This group of inhibitors was constituted by linear primary diamines of increasing length, ranging from 3 to 12 carbon atoms. These compounds, lacking secondary amino groups, were good competitive inhibitors of MPAO activity, in agreement with the idea that the MPAO catalytic tunnel represents a favorable environment for the binding of aliphatic chains of variable length (*11*). The inhibitory activity (Table 1) increased with the number of methylene groups, showing two maxima corresponding to 1,8-diaminooctane and 1,12-diaminododecane, which display the same chain length of the physiological substrates spermidine and spermine, respectively.

Agmatine, G3, and G3 Analogues. Agmatine (4-amino-1-guanidobutane), G3 (*N*-prenylagmatine), and G3 analogues (Figure 2) competitively inhibited spermine and spermidine oxidation catalyzed by MPAO (*12*, *14*). The presence of a guanidino moiety did not lead to changes in the affinity of the inhibitors for MPAO, as indicated by the K_i value determined for agmatine as compared to that for a linear diamine of comparable length [i.e., 1,6-diaminohexane (Table 1)]. On the contrary, addition of a hydrophobic substituent to one of the terminal nitrogen atoms of the agmatine guanidino group greatly increased the inhibitory activity. In fact, compounds bearing hydrophobic substituents on the guanidino group, such as G3 and Ro1−5, exhibited higher affinity for MPAO with respect to agmatine (Table 1). This result may

be explained by taking into account the stereoelectronic properties of the MPAO catalytic tunnel which provides a solvent-protected environment allowing hydrophobic interactions between ligand aliphatic carbons and aromatic side chains (*9*). In particular, a large hydrophobic patch was observed close to the large opening of the MPAO catalytic tunnel, mainly formed by the side chains of Trp60, Phe89, Tyr165, and Tyr169 (Figure 1). Furthermore, G3 and G3 analogues, such as Ro4 and Ro5, presenting a prenyl group as a substituent on the guanidino moiety exhibited the highest inhibitory activity toward MPAO. In these cases, the presence of a prenyl substituent on the guanidino moiety seemed to be the major determinant of the inhibitory activity, suggesting that the prenyl group can be bound with high affinity in a hydrophobic pocket of the MPAO active site.

On the other hand, the simultaneous presence of two terminal guanidino moieties, both bearing prenyl substituents, made the resulting compound (Ro6) less effective in inhibiting MPAO.

Guazatine. Among the known PAO inhibitors, guazatine exhibited the longest linear chain with two terminal guanidino groups. This compound strongly inhibited MPAO, with a K_i value of 7.5 nM (*12*), thus representing the most powerful plant PAO inhibitor. The strong reactivity of guazatine was likely related to two main factors: (1) the presence of long alkyl chains which can establish extensive hydrophobic interactions with the aromatic side chains lining the MPAO catalytic tunnel and (2) the presence of a secondary amino group which is able to interact strongly with both Glu62 and Glu170, with the hydroxy group of Tyr298, and with the main chain carbonyl group of Tyr169, as observed in the available crystal structure of the MPAO−guazatine complex (*11*). An additional structural determinant that is important for the binding of guazatine to MPAO was represented by the guanidino groups that in their protonated form were able to establish cation−π interactions with the aromatic residues of the catalytic tunnel (see below).

Docking Simulations

The process recognition of the Ro inhibitors by MPAO has been simulated through a computational protocol consisting of molecular docking, conformational analysis, and energy minimization of the studied compounds inside the U-shaped catalytic tunnel. For this aim, the reliability of the docking protocol was first tested by simulations of the process of recognition of 1,8-diaminooctane by MPAO, and comparison of the modeled complex with the available three-dimensional structure. 1,8-Diaminooctane has been chosen as the probe structure instead of guazatine or other compounds, because of its structural properties (size and overall length) which are similar to those of the inhibitors analyzed in this study.

The process of recognition of substrates and inhibitors by MPAO active site is not yet fully understood, and in particular, an open issue is represented by the protonation state of the substrates and inhibitors within the tunnel. On the basis of these considerations, we have performed molecular docking simulations of inhibitors in both their protonated and unprotonated forms.

Docking of 1,8-Diaminooctane. The procedure used to simulate the recognition process of the charged 1,8-diaminooctane was able to identify, among all the theoretical lowest-energy structures that were found, MPAO−1,8-diaminooctane complexes very similar to the experimental X-ray structure. In fact, two of the docking geometries of 1,8-diaminooctane collected inside an energy window of ~8 kcal/mol exhibited orientations very similar to the two alternate conformers observed in the X-ray structure. Described in detail, the lowest-energy conformer resulting from docking simulations is positioned toward the narrow entrance of the tunnel (Figure 3), showing a terminal ammonium group located inside a pocket mainly defined by Ser404 and Asn437, and contracting hydrogen bonds with the backbone carbonyl group of both residues. The second ammonium group at the opposite molecular edge contacts by hydrogen bonds the carboxy moiety of both the Glu62 and Glu170 amino acids. The root-mean-square deviation (rmsd) of this conformer with respect to the corresponding experimentally determined conformation of 1,8-diaminooctane is 0.8 Å. Alternately, one of the terminal ammonium groups of the second conformer is accommodated in a pocket near the large entrance, constituted by Phe89 and Tyr169 (Figure 4). It is involved in a network of hydrogen bonds with the backbone carbonyl group of Tyr169, with the carboxy group of Glu170, and with the water molecule 94, in turn forming a bridge to the carbonyl group of Tyr165. The opposite ammonium group makes contact with the carboxy side chain of both Glu62 and Glu170. A comparison between the second docked confomer of the inhibitor and the corresponding iso-oriented conformation found in the X-ray structure showed an rmsd value of 1.0 Å. Moreover, it is important to note that several of the interactions found in the experimental MPAO−1,8-diaminooctane complex were also predicted by

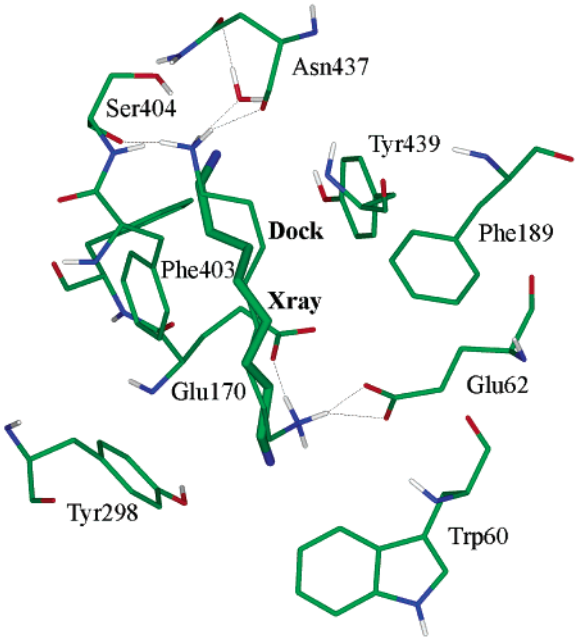

FIGURE 3: Comparison between the X-ray conformation of 1,8-diaminooctane oriented toward the narrow entrance of the catalytic tunnel (thick lines, without any hydrogen atom, labeled Xray) and the iso-oriented conformation found through docking simulations (thin lines, hydrogen atoms on the terminal ammonium groups, labeled Dock). The root-mean-square deviation (rmsd) between atomic coordinates was found to be 0.8 Å. For the sake of clarity, only few important amino acids were reported. Hydrogen bond contacts are represented with black thin dotted lines.

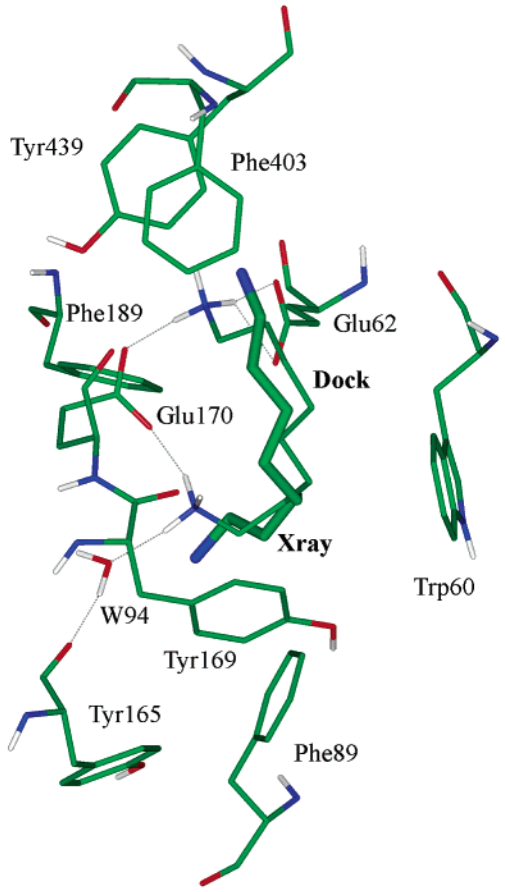

FIGURE 4: Comparison between the X-ray conformation of 1,8-diaminooctane oriented toward the large entrance of the catalytic tunnel (thick lines, without any hydrogen atom, labeled Xray) and the iso-oriented conformation found through docking simulations (thin lines, hydrogen atoms on the terminal ammonium groups, labeled Dock). The root-mean-square deviation (rmsd) between atomic coordinates was found to be 1.0 Å. For the sake of clarity, only few important amino acids were reported. Hydrogen bond contacts are represented with black thin dotted lines. W94 is water molecule 94.

the docking model, such as those involving the ammonium groups of the inhibitor and Glu62 or water molecule 94.

Molecular docking simulations on the uncharged form of 1,8-diaminooctane were also performed to investigate the influence of the protonation state of the inhibitor in defining the interactions with MPAO. Like what was observed for the protonated form of the inhibitor, different orientations were found, some of them resembling the conformations described in the X-ray structure. However, conformers resulting from docking simulations of the unprotonated inhibitor were characterized by a marked increase in the rmsd values. In fact, a comparison between the coordinates of the first and second conformers with the corresponding orientations of 1,8-diaminooctane found in the X-ray structure showed rmsd values of 1.7 and 1.0 Å, respectively. Moreover, some of the crucial interactions found between the charged ligand and the enzyme, such as the hydrogen bond involving water molecule 94 at the entrance of the catalytic tunnel, were lost with the uncharged 1,8-diaminooctane.

Analysis of the computationally generated MPAO−1,8-diaminooctane complexes led to two main suggestions. (1) Docking simulations performed with the protonated form of 1,8-diaminooctane resulted in good agreement with experimental data, at variance with the results obtained with the unprotonated form of the inhibitor. On this basis and taking into account results from GRID calculations (see below), we suggest the protonated form of the inhibitors as the chemical species that is able to interact better with the catalytic tunnel of MPAO. (2) The molecular docking/conformational search/energy minimization protocol that was used was able to identify conformers of the inhibitor very similar to those found in the X-ray structure. Moreover, the network of hydrogen bonds observed in the X-ray structure was maintained in the output docking geometries. These considerations led us to hypothesize that the computational approach can be considered as a reliable modeling procedure to be applied for finding the orientations and interactions of ligands inside the catalytic tunnel of MPAO.

General Considerations of Docking of Ro Inhibitors. Once the reliability of the docking procedure was tested, the recognition process of Ro inhibitors was simulated by applying the same protocol used for 1,8-diaminooctane. In principle, docking simulations found a double orientation (similar to that found in the complex of MPAO and 1,8-diaminooctane) of both the protonated and unprotonated inhibitors inside the catalytic tunnel of MPAO. In the first orientation, inhibitors penetrated the tunnel through their terminal ammonium group. That is, such a group was placed in the innermost portion of the tunnel, while the prenyl moiety was located at the large entrance of the tunnel. In all the inhibitors that were studied, this was the energetically preferred orientation.

On the other hand, the ammonium group of the inhibitors in the second orientation was found near the large entrance of the tunnel, while the hydrophobic terminal moiety linked to the guanidino system pointed toward the narrow entrance.

Docking of Ro4. The minimum energy complex of MPAO and Ro4 is shown in Figure 5. In this complex, the prenyl group of Ro4 was directed toward the large entrance of the tunnel, and was accommodated in a hydrophobic pocket mainly defined by aromatic residues Phe89, Tyr165, and Phe189. In addition, the carboxy group of Glu62 interacted through hydrogen bonds with both the guanidino imino group linked to the polymethylene chain and the terminal ammonium group of the inhibitor. The latter group was also involved in additional hydrogen bonds with the carboxy group of Glu170, and was located within the aromatic pocket constituted by the side chains of Tyr298, Phe403, and Tyr439. The last two residues constituted a sandwich with centroids at a distance of 8.0 Å. Distances between the ammonium nitrogen atom and the above centroids were found to be 6.0 and 3.8 Å, respectively, while the C4a atom of the flavin was 5.4 Å from the same amino nitrogen. This finding was in good agreement with the hypothesis that recognition of substrates and/or inhibitors by flavoenzymes occurred by placement of the amino group into an aromatic cage, although in MPAO extensive charge−charge interactions were observed between protein polar groups and the inhibitor cationic groups. An additional profitable interaction also involved water molecule 94, found to bridge the carbonyl group of Tyr165 and the guanidino NH_2 group of the inhibitor. The latter was also located at the proper distance for interacting by a hydrogen bond contact with the carbonyl group of Tyr169. Finally, the alkyl chain was embedded in a lipophilic pocket delimited by Tyr298 and Trp60.

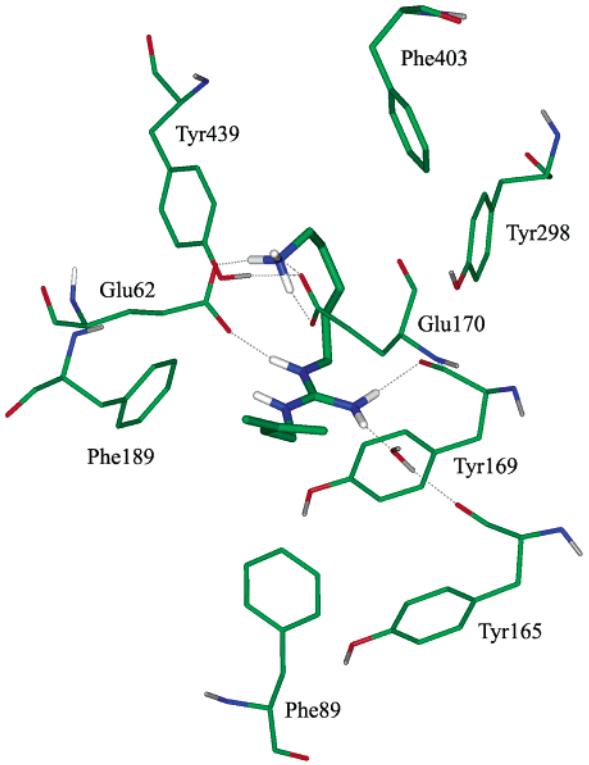

FIGURE 5: Graphical representation of the lowest-energy MPAO−Ro4 complex as obtained by docking simulations. The prenyl group of the inhibitor is oriented toward the large entrance of the catalytic tunnel, embedded in a pocket defined by aromatic residues (Phe189, Tyr169, Tyr165, and Phe89). The guanidino moiety interacts by a network of hydrogen bonds with Glu62, Tyr298, and water molecule 94, bridging the backbone carbonyl group of Tyr165. The polymethylene chain of Ro4 made lipophilic contacts with Tyr298 and Trp60. Finally, the terminal ammonium group contacts by a hydrogen bond the carboxy side chain of both Glu62 and Glu170. For the sake of clarity, only few important amino acids were reported. Hydrogen bond contacts are represented with black thin dotted lines.

Among the conformers found by the docking procedures, an orientation into the catalytic tunnel opposite to that described for the most stable complex but characterized by a slightly higher energy with respect to the global minimum (the energy difference between the two conformers has been calculated to be 4 kcal/mol) was also found. In detail, the prenyl group of the inhibitor was directed toward the narrow entrance of the catalytic tunnel, this group being located between Asn437, Ser404, and Tyr439. Moreover, both the guanidino NH group linked to the prenyl substituent and the ammonium group of Ro4 contacts the carboxy moiety of Glu170 through hydrogen bonds. In addition, the carboxy group of Glu62 shows a bifurcated hydrogen bond interaction with both the guanidino NH group bound to the polymethylene chain and the terminal ammonium group.

The Lys300/water/flavin N5 motif was conserved in all the complexes that were analyzed, in agreement with the stability of this motif observed in all the MPAO structures solved so far (*9*, *11*).

The docking approach resulted in a double orientation of the inhibitor also in the case of the MPAO-uncharged Ro4 complex. However, the inhibitor lacked some important interactions with the catalytic tunnel. In fact, the hydrophobic pocket defined by Tyr298, Tyr169, and Trp60 was not the preferred site of interaction for the hydrophobic moieties bound to the guanidino system of the inhibitors. Moreover, the terminal amino group was unable to contact via a hydrogen bond the side chain of Glu62. Finally, the hydrogen bond network involving the inhibitor and water molecule 94 was not found. Due to the lack of these essential hydrogen bonds, complexes with inhibitors in the uncharged form were not investigated further.

Other Ro Inhibitors. Lengthening the pentyl spacer of Ro4 to a hexyl chain (Ro5) did not significantly influence inhibitory activity. This was in agreement with the fact that the orientation and interactions of these inhibitors in the tunnel were very similar. The only difference consisted of the location of the alkyl chain in the lipophilic pocket defined by Tyr298, Tyr169, and Trp60, which in the case of Ro4 led to a better fit and more profitable interactions with respect to Ro5. On the other hand, compounds Ro1−Ro3, which were all characterized by different hydrophobic substituents as well as by an alkyl chain shorter than those of Ro4 and Ro5, shared similar activity values that were at least 1 order of magnitude lower than those of both Ro4 and Ro5. Docking simulations explained such activity data on the basis of the lack of important interactions. As an example, in the MPAO−Ro3 complex, the network of hydrogen bonds involving bridged water molecule 94 was disrupted, accounting for a decrease in activity of ∼60-fold with respect to that of Ro4. Moreover, in a manner different from that of the prenyl moiety of Ro4, the allyl, *p*-fluorobenzyl, and propargyl substituents of Ro1−Ro3, respectively, were characterized by shapes and steric properties that were unable to allow for a profitable filling of the Phe89−Tyr165−Phe189 hydrophobic pocket of MPAO.

Finally, the mode of binding of Ro6 to the catalytic tunnel cannot be compared to those of the remaining inhibitors, due to the different structural properties, such as the lack of the terminal ammonium group.

Cation−π Interactions in the MPAO−Inhibitor Complexes. It is well-known that aromatic amino acid residues such as Phe, Tyr, and Trp are characterized by an unusual combination of hydrophobic and quadrupolar character, allowing for an electrostatic effect usually termed a cation−π interaction (*26*). In proteins, both Arg and Lys residues were found to interact via cation−π contacts with aromatic amino acids (*27*), leading to the suggestion that both a guanidinium group (such as in guazatine and Ro derivatives) and a protonated amine (Ro and diamino MPAO inhibitors) should be able to perform such an interaction. As an example, in the MPAO−guazatine X-ray complex, one of the guanidino groups shows a stacked orientation with respect to the phenyl ring of Phe189, in agreement with data reporting that the preferred orientation of Arg guanidinium groups is parallel to aromatic rings (*27*, *28*). To quantitatively model cation−π interactions by force field-based methods, an electrostatic term (based on a directional charge−quadrupole attraction between a cation and an aromatic system) should be considered together with additional terms such as dispersion forces, charge transfer, polarizability, and induced dipoles (*28*). Only a few attempts have been made to date to reach this goal. As an example, Kollman and co-workers added a specific short-range 10−12 Lennard-Jones potential to the Amber force field (*29*), resulting in good reproducibility of *ab initio* calculations in the gas phase, but neglecting both polarization and charge transfer contributions, which are important in the cation−π interactions. On the other hand,

the Amber force field implemented in MacroModel (*32*) that we have used in our calculations also contains a similar 10−12 Lennard-Jones function to account for electrostatic interactions. As an example, Amber parametrization allowed to find an energy minimum between benzene and methylammonium ion in water, with a distance of ~3.7 Å between the nitrogen atom and the aromatic centroid, in good agreement with what found by Dougherty and co-workers (*30*). Moreover, in the Ro4 minimum energy complex, distances of ~6 and ~4 Å were found between the terminal ammonium group of the inhibitor and the aromatic moieties of Phe403 and Tyr439, respectively, values similar to those found in proteins for cation−π (Lys−Phe) interactions (*29*). An additional stacked interaction between the aromatic group of Phe169 and the guanidino group of the inhibitor was found. Finally, in the second conformer, while the guanidino moiety is sandwiched between Tyr439 and Phe403, the terminal ammonium group is at a proper distance to interact by cation−π contacts with Trp60. All these findings led to the suggestion that the Amber force field as implemented in MacroModel is able to find geometries comparable to those found in cation−π systems, and represents a helpful tool in investigating the interactions between MPAO and its inhibitors. However, further efforts are required to quantify the contribution of cation−π interactions to the binding of inhibitors and ligands to MPAO, by addition of new parameters to the force field equations or, better, by more accurate methods (i.e., *ab initio* quantum mechanical calculations) (*30*, *31*).

GRID Calculations for Further Molecular Modeling Simulations

With the purpose of validating the results obtained by docking experiments, an additional molecular modeling study using the program GRID has also been carried out. GRID is a program especially developed for the calculation of favorable binding sites on macromolecules. The program calculates the intramolecular interaction energy between the macromolecule and a probe around the macromolecule itself. By contouring the interaction energy at various levels, it is possible to locate preferred binding sites for a number of chemical groups.

In this study, we performed a series of GRID calculations to determine the most favorable binding sites for probes resembling the different functional groups of the inhibitors that were analyzed (see Experimental Procedures).

On the basis of the model derived from docking studies, favorable interaction sites for hydrophobic groups were expected to be found that corresponded to those positions of the MPAO active site where the alkyl chain and hydrophobic substituents on the guanidino group of the docked ligand lie.

GRID calculations using a hydrophobic probe indicated the presence of three preferred binding sites close to Trp60, Tyr298, and Tyr169, to Tyr165 and Phe89, and to Phe189, with the first one characterized by the most profitable interactions. Additional GRID calculations using an amino group as a probe showed two preferred binding sites close to Glu62 and Glu170 (Figure 6A) and to Ser404 and Asn405 (Figure 6B). Finally, the whole cavity of the catalytic tunnel exhibited optimal properties for interacting with an ammonium probe (Figure 7).

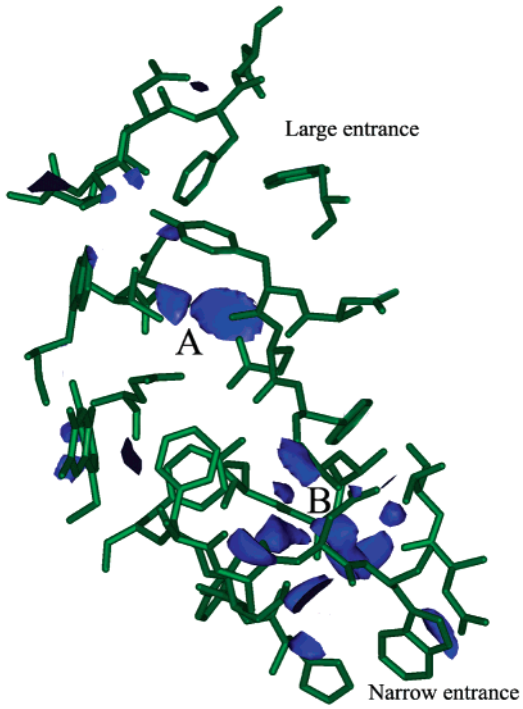

FIGURE 6: Grid interaction fields (−5 kcal/mol) calculated by using the N2 probe (an sp^3 nitrogen atom bearing two hydrogens and a lone pair) simulating a basic primary amino group. Two main regions of interaction were found between the probe and the MPAO amino acids, corresponding to the Glu62−Glu170 (A) and Ser404−Asn405 (B) residue pairs. For the sake of clarity, only amino acids defining the catalytic tunnel are shown. Moreover, the two openings of the tunnel are also evidenced.

DISCUSSION

MPAO Inhibition by Diamines and Guazatine. Linear diamines and guazatine competitively inhibited MPAO, in agreement with the hypothesis based on MPAO−inhibitor crystal structures that the MPAO catalytic tunnel allowed binding of aliphatic molecules of variable lengths (*11*). Guazatine represented the most powerful MPAO inhibitor presently available. In particular, this compound can establish strong interactions with the catalytic tunnel due to the presence of (i) long alkyl spacers interacting with aromatic amino acid side chains (Phe89, Tyr169, Phe403, and Tyr439), (ii) a secondary amino group contacting the Glu62−Glu170 pair, and (iii) guanidino moieties able to make in their protonated form a stacked cation−π interaction with aromatic residues (such as Phe189), as evidenced by the X-ray structure of the MPAO−inhibitor complex (*11*). With regard to diamines, their activity increased with the number of methylene groups, showing two maxima corresponding to 1,8-diaminooctane and 1,12-diaminododecane. In this regard, it is worthwhile to observe that these two compounds exhibited a distance between the two terminal amino groups which is comparable to that of the physiological substrates, i.e., spermidine and spermine, thus being allowed to establish stronger interactions with specific groups lining the catalytic tunnel.

Guanidino Class of Inhibitors and the Role Played by the Hydrophobic Substituent in MPAO Inhibition. Analysis of the enzyme inhibition properties exhibited by agmatine, G3, and G3 analogues pointed to the presence of a hydrophobic substituent as the main determinant of inhibitory activity. In fact, while the occurrence of a guanidino moiety did not

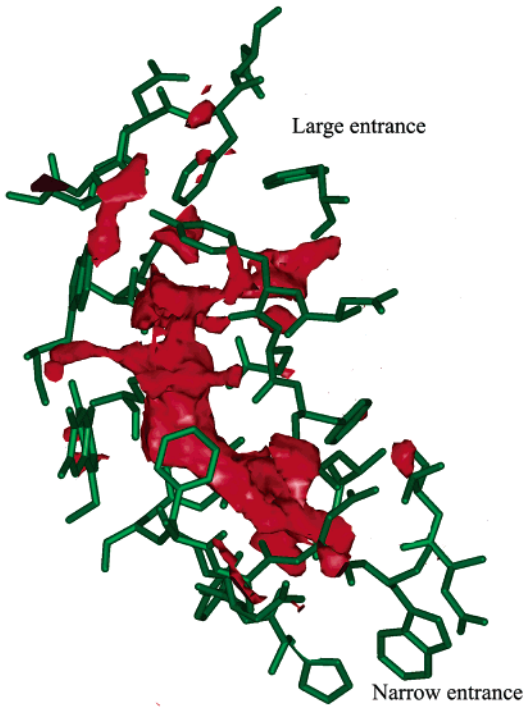

FIGURE 7: Grid interaction fields (−12 kcal/mol) calculated by using the N3+ probe (an sp^3 nitrogen atom bearing three hydrogens) simulating an ammonium group. The whole internal surface of the catalytic tunnel showed good interactions with the probe. For the sake of clarity, only amino acids defining the catalytic tunnel are shown. Moreover, the two openings of the tunnel are also evidenced.

affect the binding activity of the ligands for the enzyme, as indicated by the K_i values of agmatine versus 1,6-diaminohexane, the addition of a hydrophobic substituent to one of the terminal nitrogen atoms of the agmatine guanidino group greatly increased the inhibitory activity, as in the case of G3 and Ro1−Ro5. Moreover, variation of the length of the aliphatic chain without a change in the guanidino moiety (compare K_i values of G3 vs those of Ro4 and Ro5) did not influence the ligand binding properties, further confirming the main role played by the hydrophobic substituent. This observation can be rationalized on the basis of the MPAO X-ray structure, in which a large hydrophobic patch near the large opening of the tunnel, mainly formed by the side chains of Trp60, Phe89, Tyr165, and Tyr169, was observed. The higher affinity exhibited by G3, Ro4, and Ro5 (bearing a prenyl group) in comparison to those of Ro1−Ro3 (bearing different hydrophobic substituents) was in agreement with the presence in MPAO of a pocket within the hydrophobic patch that is able to bind the prenyl group with high affinity, as also evidenced through molecular modeling simulations. The less effective inhibitor belonging to this class of molecules was represented by Ro6, a compound showing the simultaneous presence of two terminal guanidino moieties, both bearing prenyl substituents. In this case, the presence of two terminal prenyl substituents resulted in a molecular structure with a bulky hydrophobic group in the narrow tunnel opening area, in which no hydrophobic pocket was present. As a consequence, the inhibitor was unable to bind the guanidino group near the carbonyl oxygen atoms located in this region of the active site, as opposed to what was observed in the MPAO−guazatine three-dimensional structure (*11*).

Docking Simulation on MPAO−Ro Inhibitors. On the basis of results derived from docking simulations on MPAO−Ro inhibitors, some conclusions can be drawn.

(i) The preferred orientation of Ro inhibitors, corresponding to their lowest-energy conformer, showed the ammonium group to point toward the narrow entrance of the tunnel, while the terminal hydrophobic group was directed to the large entrance. This was in agreement with the suggestion that the large entrance to the tunnel was the preferential way to admit substrates and inhibitors into the binding site, using the driving forces exherted, at the entrance of the tunnel, by a "carboxylate ring" on the terminal amino groups of inhibitors and/or substrates (*9*). In fact, upon binding, the hydrophobic moiety of Ro inhibitors should always be oriented toward the large cavity, considering the hypothesis of the electrostatic recognition between the enzyme acidic residues and amino (or ammonium) groups of the inhibitors. On the other hand, an orientation toward the narrow opening could be possible in a recognition process involving the terminal amino group and the narrow entrance itself (containing many oxygen atoms on its surface). However, this hypothesis can be excluded on the basis of the reduced overall size of the narrow entrance, which is unable to admit into the tunnel either substrates or inhibitors.

(ii) The preferred form of Ro inhibitors inside the catalytic tunnel seemed to be characterized by both terminal ammonium groups and protonated guanidino systems. This suggestion arose from molecular docking simulations, as well as from GRID calculations. With regard to the latter, GRID calculations performed with both the amino and ammonium probes led us to find regions of profitable interactions in the innermost portion of the tunnel, near FAD and between the side chains of Glu62 and Glu170. The same region has been identified by docking simulations as the region accommodating the terminal ammonium group of the inhibitors, in both their orientations. Two additional regions that are able to accommodate the ammonium group were found by GRID to correspond with the Ser404-Asn405 sequence and with the carboxylate ring at the large entrance of the tunnel. However, such interactions were found to be more profitable in the case of the ammonium probe with respect to the amino probe.

(iii) Finally, comparison of the docking results of all the inhibitors in the protonated form showed several common interactions with portions of the catalytic tunnel reported to be important in the recognition of MPAO. In particular, (a) in the preferred orientation of the inhibitors, the hydrophobic substituents on the guanidino moiety were located inside the pocket defined by Phe189, Phe89, Trp60, Tyr169, and Tyr165. This interaction was also confirmed by GRID calculations showing very profitable interactions between a hydrophobic probe and the above-mentioned aromatic residues. Moreover, the interaction pathway of the inhibitor hydrophobic substituent with this aromatic cage was able to account for the better activity of Ro4 with respect to Ro1−Ro3. On the other hand, inhibitors in the unprotonated form were found to be unable to interact with this hydrophobic pocket. (b) In the X-ray structure, water molecule 94 bridged the 1,8-diaminooctane nitrogen atom near the large entrance of the tunnel and the carbonyl group of Tyr165. A similar network of hydrogen bonds was found involving the guanidino NH2 group of the inhibitors in their preferred orientation

within the binding site. Moreover, the lack of this interaction in the complexes with Ro2 and Ro5 could explain their decreased activity with respect to Ro1 and Ro3 and to Ro4, respectively. (c) The side chain of Glu62 has been reported to be a crucial element in orienting substrates into the catalytic tunnel of MPAO. Docking simulations showed the terminal ammonium group of all inhibitors involved in hydrogen bond contacts with this residue in both the orientations into the tunnel. On the contrary, the unprotonated inhibitors were in several cases unable to contact Glu62 with their terminal amino group. (d) Structural determinants of the Ro inhibitors (i.e., guanidinium and ammonium groups) are involved in contacts with MPAO residues comparable to the cation$-\pi$ interactions.

In conclusion, the results presented here predicted that both diamino and aminoguanidino inhibitors of MPAO interact with the catalytic tunnel of the enzyme in their protonated form. Moreover, the preferential orientation of such inhibitors was reported, showing the hydrophobic terminal moiety interacting with an aromatic cage of the enzyme and the ammonium group located in a binding pocket constituted by acidic residues.

Taken together, the results illustrate that a dominant role in defining the inhibitory activity is played by the orientation of inhibitors within the MPAO catalytic tunnel. On the other hand, the proper positioning of the inhibitors within the tunnel, that is, the interactions between the chemical features of the inhibitors and the active site residues, should be considered a fine-tuning mechanism for inhibitory activity. In such a context, activity data of some MPAO inhibitors were rationalized on the basis of the enzyme−inhibitor interactions found in the binding model proposed in this paper.

REFERENCES

1. Federico, R., and Angelini, R. (1991) Polyamine catabolism, in *Biochemistry and Physiology of Polyamines in Plants* (Slocum, R. D., and Flores, H. E., Eds.) pp 41−56, CRC Press, Boca Raton, FL.
2. Cervelli, M., Polticelli, F., Federico, R., and Mariottini, P. (2003) Heterologous expression and characterization of mouse spermine oxidase, *J. Biol. Chem. 278*, 5271−5276.
3. Thomas, T., and Thomas, T. J. (2001) Polyamines in cell growth and cell death: molecular mechanisms and therapeutic applications, *Cell. Mol. Life Sci. 58*, 244−258.
4. Ha, H. C., Woster, P. M., Yager, J. D., and Casero, R. A. (1997) The role of polyamine catabolism in polyamine analogue-induced programmed cell death, *Proc. Natl. Acad. Sci. U.S.A. 94*, 11557−11562.
5. Hohl, M., Greiner, H., and Schopfer, P. (1995) The cryptic-growth response of maize coleoptiles and its relationship to H_2O_2-dependent cell wall stiffening, *Physiol. Plant. 94*, 491−498.
6. Yoda, H., Yamaguchi, Y., and Sano, H. (2003) Induction of hypersensitive cell death by hydrogen peroxide produced through polyamine degradation in tobacco plants, *Plant Physiol. 132*, 1973−1981.
7. Schopfer, P. (1996) Hydrogen peroxide-mediated cell-wall stiffening in vitro in maize coleoptiles, *Planta 199*, 43−49.
8. Cona, A., Cenci, F., Cervelli, M., Federico, R., Mariottini, P., Moreno, S., and Angelini, R. (2003) Polyamine oxidase, a hydrogen peroxide-producing enzyme, is up-regulated by light and down-regulated by auxin in the outer tissues of the maize mesocotyl, *Plant Physiol. 131*, 803−813.
9. Binda, C., Coda, A., Angelini, R., Federico, R., Ascenzi, P., and Mattevi, A. (1999) A 30 Å long u-shaped catalytic tunnel in the crystal structure of polyamine oxidase, *Structure 7*, 265−276.
10. Cervelli, M., Cona, A., Angelini, R., Polticelli, F., Federico, R., and Mariottini, P. (2001) A barley polyamine oxidase isoform with distinct structural features and subcellular localization, *Eur. J. Biochem. 268*, 3816−3830.
11. Binda, C., Angelini, R., Federico, R., Ascenzi, P., and Mattevi, A. (2001) Structural bases for inhibition binding and catalysis in polyamine oxidase, *Biochemistry 40*, 2766−2776.
12. Federico, R., Leone, L., Botta, M., Binda, C., Angelini, R., Venturini, G., and Ascenzi, P. (2001) Inhibitior of pig liver and *Zea mays* L. polyamine oxidase: a comparative study, *J. Enzyme Inhib. 13*, 465−471.
13. Delle Monache, G., Volpe, A. R., Delle Monache, F., Vitali, A., Botta, B., De Bonnevaux, S. C., De Luca, C., Botta, M., Corelli, F., and Carmingnani, M. (1999) Further hypotensive metabolites from *Verbesina caracasana*, *Bioorg. Med. Chem. Lett. 9*, 3249−3254.
14. Corelli, F., Federico, R., Cona, A., Venturini, G., Schenone, S., and Botta, M. (2002) Solution and solid-phase synthesis of aminoalkylguanidines inhibiting polyamine oxidase and nitric oxide synthase, *Med. Chem. Res. 11*, 309−321.
15. Federico, R., Alisi, C., and Forlani, F. (1989) Properties of the polyamine oxidase from the cell wall of maize seedlings, *Phytochemistry 28*, 45−46.
16. Smith, T. A., and Barker, J. H. A. (1988) The di- and polyamine oxidase of plants, in *Progress in Polyamine Research: Novel Biochemical, Pharmacological and Clinical Aspects* (Zappia, V., and Pegg, A. E., Eds.) pp 573−587, Plenum Press, New York.
17. Dixon, M. (1953) The determination of enzyme inhibitor constants, *Biochem. J. 55*, 170−171.
18. MacroModel and BatchMin, version 4.5 (1995) Columbia University, New York.
19. Mohamadi, F., Richards, N. G. J., Guida, W. C., Liskamp, R., Caufield, C., Chang, G., Hendrickson, T., and Still, W. C. (1990) MacroModel: An Integrated Software System for Modeling Organic and Bioorganic Molecules using Molecular Mechanics, *J. Comput. Chem. 11*, 440−456.
20. Gundertofte, K., Liljefors, T., Norrby, P.-O., and Pettersson, I. (1996) A comparison of conformational energies calculated by several molecular mechanics methods, *J. Comput. Chem. 17*, 429−449.
21. InsightII, version 2000 (2000) Accelrys, Inc., San Diego.
22. Stewart, J. J. (1990) MOPAC: a semiempirical molecular orbital program, *J. Comput.-Aided Mol. Des. 4*, 1−105.
23. Still, W. C., Tempczyk, A., Hawley, R. C., and Hendrickson, T. (1990) Semianalytical treatment of solvation for molecular mechanics and dynamics, *J. Am. Chem. Soc. 112*, 6127−6130.
24. Goodford, P. J. (1985) A computational procedure for determining energetically favorable binding sites on biologically important macromolecules, *J. Med. Chem. 28*, 849−857.
25. Boobbyer, D. N. A., Goodford, P. J., McWhinnie, P. M., and Wade, R. C. (1989) New hydrogen-bond potentials for use in determining energetically favorable binding sites on molecules of known structure, *J. Med. Chem. 32*, 1083−1094.
26. Zacharias, N., and Dougherty, D. A. (2002) Cation-π interactions in ligand recognition and catalysis, *Trends Pharmacol. Sci. 23*, 281−287.
27. Tsou, L. K., Tatko, C. D., and Waters, M. L. (2002) Simple cation-π interaction between a phenyl ring and a protonated amine stabilizes an α-helix in water, *J. Am. Chem. Soc. 124*, 14917−14921.
28. Dougherty, D. A. (1996) Cation-π interactions in chemistry and biology: a new view of benzene, Phe, Tyr, and Trp, *Science 271*, 163−168.
29. Chipot, C., Maigret, B., Pearlman, D. A., and Kollman, P. A. (1996) Molecular dynamics potential of mean force calculations: a study of the toluene-ammonium π-cation interactions, *J. Am. Chem. Soc. 118*, 2998−3005.
30. Gallivan, J. P., and Dougherty, D. A. (2000) A computational study of cation-π interactions vs salt bridges in aqueous media: implications for protein engineering, *J. Am. Chem. Soc. 122*, 870−874.
31. Biot, C., Buisine, E., and Rooman, M. (2003) Free-energy calculations of protein−ligand cation−π and amino−π interactions: from vacuum to proteinlike environments, *J. Am. Chem. Soc. 125*, 13988−13994.
32. Weiner, S. J., Kollman, P. A., Case, D. A., Singh, U. C., Ghio, C., Alagona, G., Profeta, S., and Weiner, P. (1984) A new force field for molecular mechanical simulation of nucleic acids and proteins, *J. Am. Chem. Soc. 106*, 765−784.

BI036152Z